Observation of soft phonon mode in $TbFe_3(BO_3)_4$ by inelastic neutron scattering

M. S. Pavlovskiy,[1] K. A. Shaykhutdinov,[1] L. S. Wu,[2] G. Ehlers,[3] V. L. Temerov,[1]
I. A. Gudim,[1] A. S. Shinkorenko,[1] and A. Podlesnyak[2,*]

[1]*Kirensky Institute of Physics, Federal Research Center, Krasnoyarsk 660036, Russia*
[2]*Neutron Scattering Division, Oak Ridge National Laboratory, Oak Ridge, Tennessee 37831, USA*
[3]*Neutron Technologies Division, Oak Ridge National Laboratory, Oak Ridge, Tennessee 37831, USA*

(Received 16 November 2017; revised manuscript received 23 January 2018; published 28 February 2018)

The phonon dispersion in terbium iron borate $TbFe_3(BO_3)_4$ has been measured by inelastic neutron scattering in a temperature range $180 < T < 350$ K through the displacive structural transition at $T_S = 192.5$ K and studied by *ab initio* calculations. Significant, but not complete, softening of the transverse acoustic (TA) branch has been observed at the corner of the Brillouin zone (Λ point) at temperatures $T \gtrapprox T_S$, in full agreement with theoretical calculations. The TA soft mode undergoes considerable broadening at the Λ point near the transition temperature that can be attributed to the anharmonic interference between transverse acoustic and optical modes.

DOI: 10.1103/PhysRevB.97.054313

I. INTRODUCTION

Rare-earth-metal iron borates $RFe_3(BO_3)_4$ (where R is a rare-earth metal or yttrium) with the hantite structure [1] have attracted considerable attention because of a number of intriguing nonliner optical [2] and magnetic phenomena, like multiferroic properties [3] with giant magnetoelectric effect [4–6] and a spin-reorientation transition [7]. The magnetic properties are the result of interacting magnetic subsystems of iron and rare-earth-metal ions and strongly depend on the structural features. The high-temperature crystal structure of $RFe_3(BO_3)_4$ has the trigonal noncentrosymmetric space group $R32$ and features helicoidal chains of distorted FeO_6 octahedra with threefold symmetry; see Figs. 1(a) and 1(b). The FeO_6 octahedra are interconnected by RO_6 prisms and BO_3 groups. In the compounds with $R =$ Eu–Er and Y, a structural displacive phase transition $R32 \rightarrow P3_121$ has been observed on cooling. The transition temperature T_S varies in a wide range, from 88 to 450 K, depending on the rare-earth metal [8,9]. In the crystals with $R =$ La–Sm, the structural transition was not experimentally observed. At the displacive structural transition, the rotational symmetry remains invariable, whereas the translation symmetry is broken, and the primitive unit cell volume increases threefold. It should be noted that the local environment of the rare-earth-metal ion changes (point group 32 in the $R32$ phase and point group 2 in the $P3_121$ phase). Thus, the crystal electric fields (CEF) acting on a rare-earth-metal ion in the $R32$ and $P3_121$ phases are expected to be different. This leads to a difference in the low-temperature magnetic, magnetoelastic, and magnetoelectric properties of the compounds with and without displacive phase transition. Therefore, it is important to study the details of this phase transition in order to get a complete picture of the phenomena that take place in the family of rare-earth-metal ferroborate crystals.

The structure of the low-temperature phase was first determined in the $GdFe_3(BO_3)_4$ system [9]. The lattice dynamics at the center of the Brillouin zone of several $RFe_3(BO_3)_4$ compounds undergoing the phase transition $R32 \rightarrow P3_121$ was studied by Raman and infrared reflection (IR) spectroscopy [9–11]. Significant variations of IR spectra across the phase transition and a soft-mode recovery at low frequencies ($\hbar\omega < 6$–7 meV) below T_S from Raman spectra were observed. Complete information about the phonon spectra can be obtained using the inelastic neutron scattering (INS) technique. We should note that displacive structural transitions have been studied over decades in numerous compounds by INS, e.g., ferroelectric perovskites [12], Jahn-Teller systems [13,14], and compounds exhibiting martensitic transitions [15,16] (see also a comprehensive review [17]). However, to our knowledge, no INS studies have been performed so far on the lattice dynamics in iron borates. There is the only INS reference regarding the low-temperature spin dynamics of $NdFe_3(BO_3)_4$ [3]. Therefore, the lattice dynamics involving the soft phonon mode and the related displacive structural transition in $RFe_3(BO_3)_4$ remain largely unexplored to date.

Previously, we calculated the phonon spectrum of the $HoFe_3(BO_3)_4$ system in the high-temperature phase with the $R32$ space group [18]. We found an anomaly in the behavior of the transverse acoustic (TA) phonon, specifically, a dip near the Λ point of the Brillouin zone (see Table I in the appendix) atypical of acoustic branches. We demonstrated that the distortion of the $R32$ phase of holmium ferroborate by the eigenvector of this mode yields the space group $P3_121$ with three formula units, which corresponds to the structure observed experimentally below the temperature of the phase transition in this crystal.

In this work, we use INS measurements in combination with first-principles calculations to study the acoustic phonon dispersion in $TbFe_3(BO_3)_4$ through the $R32 \rightarrow P3_121$ phase transition. We show that the TA phonon softens toward zero frequency at the Λ point around T_S with decreasing

*Corresponding author: podlesnyakaa@ornl.gov

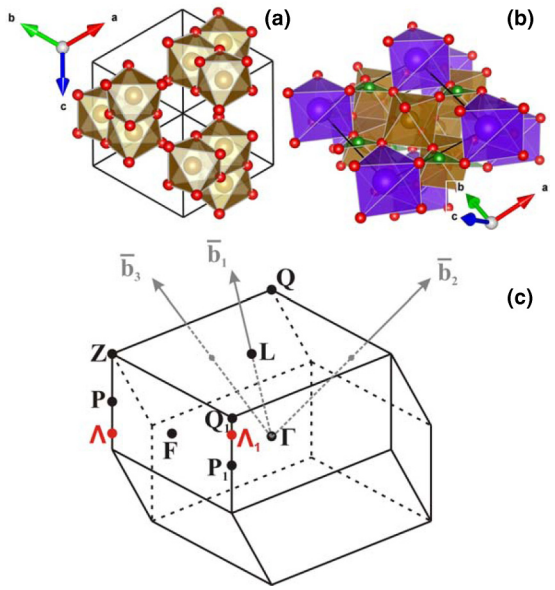

FIG. 1. Top: Schematic crystal structure of $TbFe_3(BO_3)_4$. (a) The helicoidal chains of edge-sharing FeO_6 octahedra with threefold symmetry. Tb and B atoms are omitted for clarity. (b) The FeO_6 octahedra interconnected by two kinds of BO_3 triangles (green) and RO_6 distorted prisms (violet). Bottom: (c) Brillouin zone with symmetry points and axes of the trigonal $R32$ symmetry group.

temperature. This soft-mode behavior is also well reproduced by our first-principles calculations.

II. EXPERIMENTAL

A $TbFe_3(^{11}BO_3)_4$ single crystal with a mass of 3 g was grown from flux; a more detailed description of the synthesis can be found elsewhere [19]. The sample was prepared with ^{11}B enriched to 99% to minimize the strong neutron absorption of natural boron.

Studies of the temperature dependence of the specific heat $C(T)$ were carried out on a ∼5 mg crystal using a relaxation technique on a PPMS-6000 (Quantum Design). To increase the accuracy, the measurements were carried out in two steps. At the first step, the contribution of the applied thermoglue was measured, and in the second step the sample was added. The heat capacity of the sample was calculated from the obtained data.

The single-crystal INS measurements were performed at the Cold Neutron Chopper Spectrometer (CNCS) [20,21] at Oak Ridge National Laboratory. The $TbFe_3(BO_3)_4$ single crystal was oriented in the $(H0L)$ scattering plane (throughout the paper, hexagonal lattice settings are being used). The data were collected using a fixed incident neutron energy of 12.0 meV in "high flux" (coarse resolution) mode. In this configuration, an energy resolution of $\Delta_0 = 0.38(1)$ meV full width half maximum (FWHM) was obtained for elastic scattering. The data were recorded while rotating the sample in 2° steps, over a wide range of angles, at temperatures $T = 350$, 250, 198, and 180 K. Additional measurements were performed with vanadium to allow the correction of the raw data for detector efficiency using standard procedures. To quantify the background signal from the sample environment, the INS spectra from the empty sample holder were also measured at the same temperatures. The data were combined to generate the four-dimensional scattering function, $S(\mathbf{Q},\hbar\omega)$, where $\mathbf{Q}$ is the momentum transfer, using standard software [22]. The HORACE software package [23] was used for data analysis and visualization.

Lattice dynamics calculations were carried out using the projector-augmented wave (PAW) method [24] within density functional theory (DFT), as implemented in the VASP code [25]. We used the generalized gradient approximation (GGA) functional with Perdew-Burke-Ernzerhof (PBE) parametrization [26]. Electronic configurations were chosen as follows: Tb, $5p^6 5d^1 6s^2$; Fe, $3d^7 4s^1$; B, $2s^2 2p^1$; and O, $2s^2 2p^4$. Tb $4f$ electrons were assumed as frozen in the core. The plane-wave cutoff was set at 600 eV. The size of the k-point mesh for Brillouin zone, based on the Monkhorst-Pack scheme [27], was $7 \times 7 \times 7$. The GGA+U calculations within Dudarev's approach [28] were performed by applying a Hubbard-like potential for Fe d states. The phonons were calculated by constructing a supercell ($2 \times 2 \times 2$) and calculating the force constants using the small displacement method implemented in PHONOPY [29].

III. RESULTS AND DISCUSSION

At high temperatures, $TbFe_3(BO_3)_4$ adopts a trigonal structure that is described with the $R32$ space group. The unit cell contains three formula units, and the room-temperature lattice constants are $a = 9.552(1)$ Å and $c = 7.574(1)$ Å (hexagonal). The primitive cell is a rhombohedron with the lattice constant $a_r = 6.065(1)$ Å and $\alpha = 103.9(1)°$. In the case of $\alpha > 90°$, the Brillouin zone is a dodecahedron, depicted in Fig. 1(c). The coordinates of the critical points and conversion matrix from rhombohedral (hR) to hexagonal (hP) crystal axes are presented in the Appendix.

Phonon band structure calculations give a reliable criterion to check for the structure stability and for unstable phonon modes (modes with an imaginary frequency). Figure 2 represents the calculated phonon spectrum along high-symmetry directions in the Brillouin zone and partial density of states of the constituent elements in the high-temperature $R32$ phase. In borate oxides, two types of B-O coordination polyhedra are commonly present, planar triangular BO_3 and/or BO_4 tetrahedra. As indicated in Fig. 1(b), the crystal structure of $TbFe_3(BO_3)_4$ is characterized by two BO_3 groups: equilateral BO_3 and isosceles BO_3 (see Ref. [9] for details). The highest vibrational frequency (∼150 meV) originates primarily from vibrations of boron ions in the ab plane, i.e., in the triangular plane along the B-O bonds. The phonons observed around ∼120 meV correspond to oxygen vibrations in the ab plane, including branches associated with the breathing modes at the center of the Brillouin zone. The energy band between 70 and 90 meV arises from out-of-plane vibrations of oxygen and boron ions. The low-frequency part of the spectrum (<20 meV) is dominated by Tb ion vibrations.

Unstable transverse acoustic (TA) modes were found in the vicinity of the Λ and Λ_1 points. The distortion of the $R32$ crystal structure along the eigenvector of the unstable mode at the Λ (or Λ_1) point leads to a phase with a space group

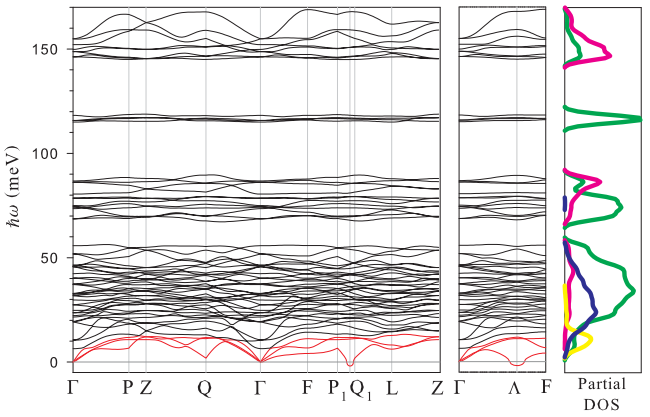

FIG. 2. Theoretically calculated phonon spectrum along high-symmetry directions of the first Brillouin zone of $TbFe_3(BO_3)_4$ in the $R32$ structure (the Λ_1 point is between P_1 and Q_1). Imaginary frequencies of the unstable modes are shown in the real negative frequency range. The acoustic branches are marked in red. The right side of the figure shows the partial phonon density of states of the constituent elements: terbium, yellow; iron, blue; oxygen, green; boron, pink.

symmetry $P3_121$. This agrees well with the group-theoretical analysis [40], which concludes that the $R32 \rightarrow P3_121$ phase transition involves a distortion which has the symmetry of the two-dimensional representation Λ_3 and is associated with one of its components (Λ_3 contains two vectors, $\mathbf{k_1} = 1/3(-2\mathbf{b_1} + \mathbf{b_2} + \mathbf{b_3})$ and $\mathbf{k_2} = 1/3(2\mathbf{b_1} - \mathbf{b_2} - \mathbf{b_3})$ [30]). In $TbFe_3(BO_3)_4$ with natural boron isotope the structural phase transition takes place at $T_S = 192$ K [19]. This is in good agreement with our estimation of T_S taken from the DFT calculations. The full energy gain achieved by the ion displacements along the eigenvector of the soft mode is about 15 meV, that is, 174 K.

We determine the transition temperature T_S for the sample enriched with ^{11}B experimentally from the temperature dependence of the specific heat $C_p(T)$, as shown in Fig. 3. On cooling the anomaly at $T_S = 192.5$ K corresponds to the structural phase transition, in agreement with the data for $TbFe_3(BO_3)_4$ with natural boron [19]. The low-temperature anomaly is

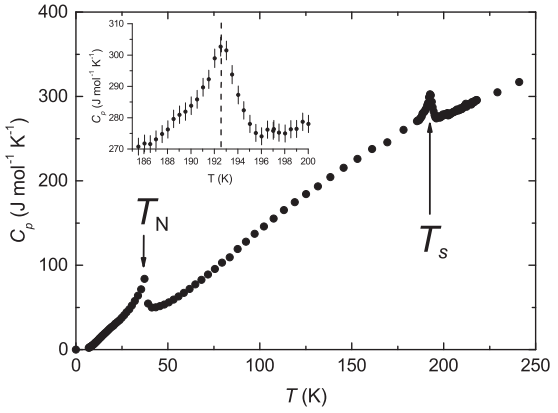

FIG. 3. Temperature dependence of the specific heat of $TbFe_3(BO_3)_4$. The arrows show the antiferromagnetic $T_N = 37.4(1)$ K and structural $T_S = 192.5(1)$ K transition temperatures.

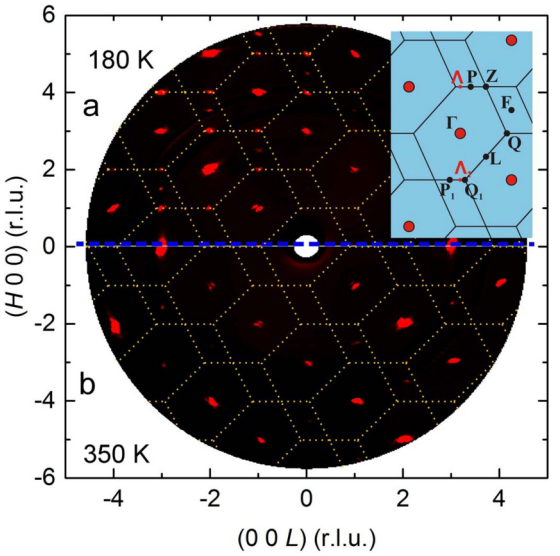

FIG. 4. Reciprocal $(H0L)$ map of $TbFe_3(BO_3)_4$ measured on CNCS at $T = 180$ K (a) and 350 K (b). Data are elastic scattering only, integrated over the energy transfer range ± 0.5 meV. The dotted lines represent the intersection of the Brillouin zone with the $K = 0$ plane for the high-temperature structure. The inset shows the symmetry points of the Brillouin zone with the $R32$ structure. Axis values are in reciprocal lattice units (r.l.u.). Note that not all weak reflections are clear visible due to instrumental constraints.

associated with the magnetic phase transition [3,31], which is outside the scope of the present article.

Figure 4 shows a comparison of the neutron-diffraction intensity maps in the $(H0L)$ scattering plane at temperatures above and below the structural transition. At $T = 180$ K, a series of additional structural reflections appears, confirming a phase transition to a less symmetric space group. All additional structural peaks can be indexed using the space group $P3_121$, in full agreement with previous studies [9,19].

We concentrated our INS study on the temperature dependence of the lowest TA phonon branch, which according to the DFT calculations has a significant anomaly in the vicinity of the Λ point. In order to compare the INS spectra taken at different temperatures, we transformed the structure factor $S(\mathbf{Q},\hbar\omega)$ to the imaginary dynamical susceptibility [32]

$$\chi''(\mathbf{Q},\hbar\omega) = \frac{S(\mathbf{Q},\hbar\omega)}{n(\hbar\omega)+1} = S(\mathbf{Q},\hbar\omega)(1 - e^{-\hbar\omega/k_B T}), \quad (1)$$

where $n(\hbar\omega)$ is the Bose factor and k_B is the Boltzman constant.

Figure 5 shows the dispersion of the acoustic branches in the $\Gamma \rightarrow \Lambda$ direction of the Brillouin zone at temperatures $T = 350$, 250, 198, and 180 K. As can be seen in Fig. 5(a), the lowest-frequency TA phonon dispersion exhibits a pronounced dip at the Λ point already at $T = 350$ K, the highest temperature that was measured. At $T = 250$ K, the observed spectrum does not reveal noticeable changes. The lowest-frequency mode shifts down by 0.8 meV and remains well shaped. The phonon line is softened and broadened progressively when the temperature is lowered to $T = 198$ K. The intensity of the TA phonon mode is distributed down toward zero energy transfer. The details of the energy broadening of the soft inelastic peak are best illustrated by cuts at constant $Q = \Lambda$ as shown in

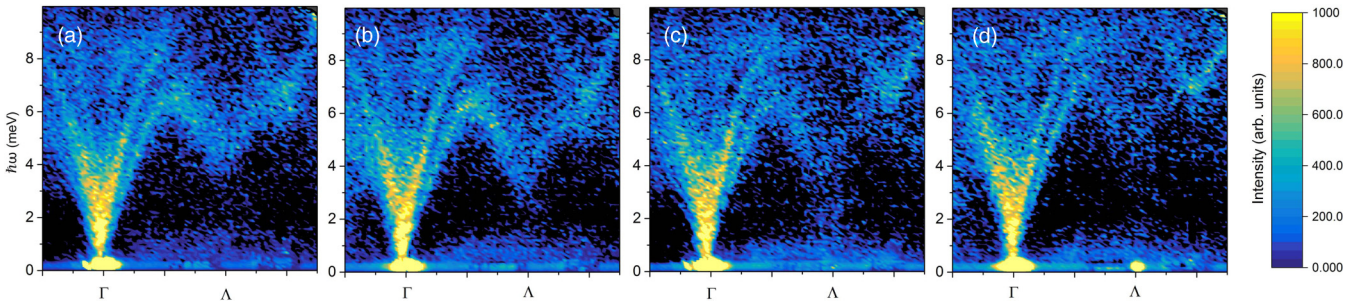

FIG. 5. Color maps of the inelastic neutron scattering spectra measured in $TbFe_3(^{11}BO_3)_4$ single crystal at $T = 350$ (a), 250 (b), 198 (c) and 180 K (d), showing the acoustic phonon dispersion along the $\Gamma \rightarrow \Lambda$ direction, where lower and higher energy branches are assigned to two transverse acoustic (TA) and longitudinal acoustic (LA) modes, respectively. The integration depth along the K and L directions is ± 0.1 r.l.u.

Fig. 6(a). We fit the obtained spectra at different temperatures to phonon modes modeled as a damped harmonic oscillator,

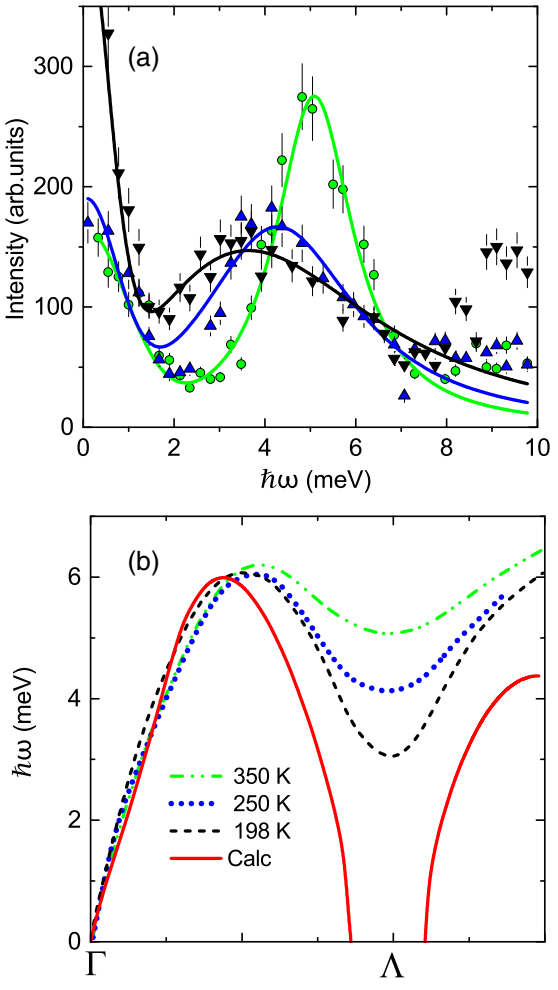

FIG. 6. (a) INS spectra of the soft phonon mode at the Λ point at different temperatures, obtained by integration in a **q** range $H,K,L < 0.1$ r.l.u. The solid curves are fits to the data by a damped harmonic oscillator model (2). The elastic line was fitted by a Gaussian function. (b) Comparison between experimentally observed (green, 350 K; blue, 250 K; black, 198 K) and calculated (red line) TA phonon dispersion along the $\Gamma \rightarrow \Lambda$ crystal orientation, at different temperatures.

whose intensity is [32,33]

$$I(\omega) \propto \frac{1}{\omega_q}\left[\frac{\Gamma_q}{\left[(\omega-\omega_q)^2+\Gamma_q^2\right]} - \frac{\Gamma_q}{(\omega+\omega_q)^2+\Gamma_q^2}\right], \quad (2)$$

where Γ_q is the damping constant and q is the reduced wave vector. The full lines in Fig. 6(a) correspond to fits to Eq. (2). We did not use a convolution with the instrumental resolution function since the CNCS resolution Δ_0 is much smaller than the obtained Γ_q values.

Three significant effects are seen in the vicinity of the structural transition at $T \gtrapprox T_S$. (i) The soft-mode frequency remains finite; that is, the TA branch does not soften completely. (ii) Elastic scattering (central peak) develops as $T \rightarrow T_S$ [16]. It is due to local clusters of the new low-temperature phase which form at temperatures above T_S. As one can see in Figs. 5 and 6(a), the elastic intensity drastically increases as the transition temperature T_S is approached. At the same time, the width of the elastic line decreases with temperature decreasing. A Gaussian fit of the peak yields a FWHM values of 2.20(5), 1.71(5), and 1.29(3) meV for the temperatures 350, 250, and 198 K, respectively. Finally, at temperatures below T_S the Λ point becomes a new Bragg position of the $P3_121$ structure [see Fig. 5(d)]. The acoustic phonons of the low-temperature phase were not clearly resolved, apparently due to low intensity. Note that the original soft-mode theory [34] explains neither (i) nor (ii). According to that model, the lattice displaces spontaneously at T_S due to an unstable phonon with an effective frequency $\omega_S^2 = (T - T_S) \rightarrow 0$ as $T \rightarrow T_S$. Although this was observed experimentally, at least in some certain materials [35], the standard soft-mode model is not applicable to our case. The central peak anomaly was explained in the Landau-type phenomenological theory developed by Krumhansl and Gooding [36]. These authors showed that low-frequency phonon modes do not necessarily need to soften completely in order to drive the structural transition. Their main idea is that if the phonon mode is not completely softened at T_S, a first-order phase transition takes place and the instability itself is not dynamic but thermodynamic. Namely, the free energy for a single-component order parameter η can be written in the form $F = (A/2)\eta^2 + (B/3)\eta^3 + (C/4)\eta^4$. If B is negative, and both A and C are positive, free energy F can develop minima not only at $\eta = 0$, but also at some finite η_1. When $F(\eta = 0) = F(\eta_1)$ a first-order phase transition takes

place with discontinuous jump in η. Thus, in both phases, the curvature of F is upward and finite, implying that the mode frequencies in either phase are nonzero and that both lattices are dynamically stable. Along this line, many other researchers studied experimentally and theoretically this concept in connection with the soft-mode transformation mechanism (see, for instance, [16,37,38] and references therein).

(iii) The TA phonon mode undergoes considerable broadening in the vicinity of the Λ point near the transition temperature. A damping $\Gamma = 2\hbar/\tau$ reflects an inverse relaxation time, and overdamping occurs in the case of $\hbar\omega < \Gamma$. At $T = 350$ K, the phonon peak is well shaped and not overdamped [see Fig. 6(a)]. The values of energy $\hbar\omega$ and the Γ_Λ of the TA mode, obtained by fitting to Eq. (2), are 5.09(5) and 1.0(1) meV, respectively. At $T = 250$ K, the corresponding values are $\Gamma_\Lambda = 2.2(1)$ and $\hbar\omega = 4.25(6)$ meV. As the temperature approaches T_S, the soft phonon mode becomes overdamped, with $\Gamma_\Lambda(198K) = 3.9(1)$ and $\hbar\omega = 3.1(1)$ meV. A damping can be attributed to the interaction (anharmonic interference) between transverse acoustic and transverse optical (TO) modes [39]. Only three symmetry types of the vibrations are possible at the boundary point Λ of the Brillouin zone in the $R32$ phase of $TbFe_3(BO_3)_4$ (see, e.g., Ref. [40]), and all three acoustic modes at this point have different symmetries. Therefore, if there is an unstable optical mode close to the acoustic ones, then its symmetry will necessarily coincide with the symmetry of the vibration of one of the acoustic modes at this point. When the temperature is lowered, the frequency of the soft optical mode gradually decreases. The TO and TA modes of the same symmetry cannot cross each other, implying the anharmonic interaction between two modes. Note that we were not able to unambiguously determine the dispersion curves corresponding to the low-energy optical branches even though a clear increase of the inelastic intensity at the high-energy side, $\hbar\omega > 8$ meV, in the vicinity of the structural transition $T = 198$ K could be due to softening of the TO modes; see Fig. 6(a). This question remains open for further studies.

IV. CONCLUSION

To conclude, the lattice dynamics in a $TbFe_3(BO_3)_4$ crystal has been studied by inelastic neutron scattering and first-principles calculations. The existence of a predicted soft TA mode with an energy minimum at the Λ point in the Brillouin zone, at the critical temperature, was experimentally confirmed. We find a significant energy broadening of the TA mode, which highlights the important role of anharmonicity effects for the displacive phase transition. Further INS measurements could clarify the role of unstable optical modes in the displacive phase transition of rare-earth-metal iron borates.

TABLE I. Symmetry k points of rhombohedral lattice [41].

$\times b_1$	$\times b_2$	$\times b_3$		$\times b_1$	$\times b_2$	$\times b_3$	
0	0	0	Γ	ν	$\nu-1$	$\nu-1$	P_1
1/2	−1/2	0	F	η	η	η	Q
1/2	0	0	L	$1-\eta$	$-\eta$	$-\eta$	Q_1
$1-\nu$	$-\nu$	$1-\nu$	P	1/2	–1/2	1/2	Z
1/3	–2/3	1/3	Λ	2/3	–1/3	–1/3	Λ_1

$\eta = 1/[2\ \tan^2(\alpha/2)] \approx 0.306$ $\nu = 3/4 - \eta/2 \approx 0.597$

ACKNOWLEDGMENTS

This research used resources at the Spallation Neutron Source, a DOE Office of Science User Facility operated by Oak Ridge National Laboratory. L.S.W. was supported by the Laboratory Directed Research and Development Program of Oak Ridge National Laboratory, managed by UT-Battelle, LLC, for the US DOE. The work was funded by RFBR, Government of Krasnoyarsk Territory, Krasnoyarsk Region Science and Technology Support Fund according to Research Project No. 16-42-243039.

APPENDIX: THE COORDINATES OF HIGH-SYMMETRY POINTS IN RHOMBOHEDRAL LATTICE

The shape of the Brillouin zone shown in Fig. 1(c) arises in the case of a direct lattice with a primitive cell in the form of a rhombohedron with an angle $\alpha > 90^\circ$ (in the case of $\alpha < 90^\circ$, the Brillouin zone takes a completely different form). The coordinates of the critical points are presented in Table I.

The vectors of the reciprocal lattice b_1, b_2, and b_3 pass through the centers of the upper three faces (the boundary point L and its symmetrically equivalent points), which are rhombuses. The threefold rotation axis passes through the center of the zone (at the Γ point) and the boundary point Q. The three twofold rotation axes pass through the center of the zone (at the Γ point) and through the centers of the side faces (the boundary point F and its symmetrically or translationally equivalent points), which are parallelograms. The Λ point related to the structural phase transition is located on the edge of the zone between the points Q and Z, and very close to the point Q. The points Λ and Λ_1 are turned into each other by the twofold rotation axis.

Conversion between the rhombohedral (hR) and hexagonal (hP) crystal systems can be done using the rotation matrix

$$\mathrm{hR}\begin{pmatrix} -1 & 0 & 1 \\ 0 & 1 & -1 \\ -1 & -1 & -1 \end{pmatrix} = \mathrm{hP}\ .$$

[1] J. A. Campá, C. Cascales, E. Gutiérrez-Puebla, M. A. Monge, I. Rasines, and C. Ruíz-Valero, Crystal structure, magnetic order, and vibrational behavior in iron rare-earth borates, Chem. Mater. **9**, 237 (1997).

[2] X. Chen, Z. Luo, D. Jaque, J. J. Romero, J. G. Sole, Y. Huang, A. Jiang, and C. Tu, Comparison of optical spectra of Nd^{3+} in $NdAl_3(BO_3)_4$ (NAB), Nd:$GdAl_3(BO_3)_4$ (NGAB) and Nd:$Gd_{0.2}Y_{0.8}Al_3(BO_3)_4$ (NGYAB) crystals, J. Phys.: Condens. Matter **13**, 1171 (2001).

[3] S. Hayashida, M. Soda, S. Itoh, T. Yokoo, K. Ohgushi, D. Kawana, H. M. Rønnow, and T. Masuda, Magnetic model in multiferroic $NdFe_3(BO_3)_4$ investigated by

inelastic neutron scattering, Phys. Rev. B **92**, 054402 (2015).

[4] K.-C. Liang, R. P. Chaudhury, B. Lorenz, Y. Y. Sun, L. N. Bezmaternykh, V. L. Temerov, and C. W. Chu, Giant magnetoelectric effect in $HoFe_3(BO_3)_4$, Phys. Rev. B **83**, 180417(R) (2011).

[5] A. L. Freydman, A. D. Balaev, A. A. Dubrovskiy, E. V. Eremin, V. L. Temerov, and I. A. Gudim, Direct and inverse magnetoelectric effects in $HoFe_3(BO_3)_4$ single crystal, J. Appl. Phys. **115**, 174103 (2014).

[6] A. K. Zvezdin, S. S. Krotov, A. M. Kadomtseva, G. P. Vorob'ev, Y. F. Popov, A. P. Pyatakov, L. N. Bezmaternykh, and E. A. Popova, Magnetoelectric effects in gadolinium iron borate $GdFe_3(BO_3)_4$, JETP Lett. **81**, 272 (2005).

[7] A. Pankrats, G. Petrakovskii, A. Kartashev, E. Eremin, and V. Temerov, Low-temperature magnetic phase diagram of $HoFe_3(BO_3)_4$ holmium ferroborate: A magnetic and heat capacity study, J. Phys.: Condens. Matter **21**, 436001 (2009).

[8] Y. Hinatsu, Y. Doi, K. Ito, M. Wakeshima, and A. Alemi, Magnetic and calorimetric studies on rare-earth iron borates $LnFe_3(BO_3)_4$ (Ln = Y, La-Nd, Sm-Ho), J. Solid State Chem. **172**, 438 (2003).

[9] S. A. Klimin, D. Fausti, A. Meetsma, L. N. Bezmaternykh, P. H. M. van Loosdrecht, and T. T. M. Palstra, Evidence for differentiation in the iron-helicoidal chain in $GdFe_3(BO_3)_4$, Acta Crystallogr. B **61**, 481 (2005).

[10] D. Fausti, A. A. Nugroho, P. H. M. van Loosdrecht, S. A. Klimin, M. N. Popova, and L. N. Bezmaternykh, Raman scattering from phonons and magnons in $RFe_3(BO_3)_4$, Phys. Rev. B **74**, 024403 (2006).

[11] V. S. Kurnosov, V. V. Tsapenko, L. N. Bezmaternykh, and I. A. Gudim, IR spectroscopy of the low-frequency phonon spectrum of the $TbFe_3(BO_3)_4$ single-crystal, Low Temp. Phys. **40**, 1087 (2014).

[12] S. M. Shapiro, J. D. Axe, G. Shirane, and T. Riste, Critical neutron scattering in $SrTiO_3$ and $KMnF_3$, Phys. Rev. B **6**, 4332 (1972).

[13] R. J. Elliott, G. A. Gehring, A. P. Malozemoff, S. R. P. Smith, W. S. Staude, and R. N. Tyte, Theory of co-operative Jahn-Teller distortions in $DyVO_4$ and $TbVO_4$ (Phase transitions), J. Phys. C **4**, L179 (1971).

[14] R. J. Birgeneau, J. K. Kjems, G. Shirane, and L. G. Van Uitert, Cooperative Jahn-Teller phase transition in $PrAlO_3$, Phys. Rev. B **10**, 2512 (1974).

[15] W. Petry, Phonons at martensitic phase transitions of bcc-Ti, bcc-Zr and bcc-Hf, Phase Trans. **31**, 119 (1991).

[16] A. Zheludev, S. M. Shapiro, P. Wochner, A. Schwartz, M. Wall, and L. E. Tanner, Phonon anomaly, central peak, and microstructures in Ni_2MnGa, Phys. Rev. B **51**, 11310 (1995).

[17] J. F. Scott, Soft-mode spectroscopy: Experimental studies of structural phase transitions, Rev. Mod. Phys. **46**, 83 (1974).

[18] V. I. Zinenko, M. S. Pavlovskii, A. S. Krylov, I. A. Gudim, and E. V. Eremin, Vibrational spectra and elastic, piezoelectric, and magnetoelectric properties of $HoFe_3(BO_3)_4$ and $HoAl_3(BO_3)_4$ crystals, Sov. Phys. JETP **117**, 1032 (2013).

[19] C. Ritter, A. Balaev, A. Vorotynov, G. Petrakovskii, D. Velikanov, V. Temerov, and I. Gudim, Magnetic structure, magnetic interactions, and metamagnetism in terbium iron borate $TbFe_3(BO_3)_4$: A neutron diffraction and magnetization study, J. Phys.: Condens. Matter **19**, 196227 (2007).

[20] G. Ehlers, A. Podlesnyak, J. L. Niedziela, E. B. Iverson, and P. E. Sokol, The new cold neutron chopper spectrometer at the Spallation Neutron Source: Design and performance, Rev. Sci. Instrum. **82**, 085108 (2011).

[21] G. Ehlers, A. Podlesnyak, and A. I. Kolesnikov, The cold neutron chopper spectrometer at the Spallation Neutron Source: A review of the first 8 years of operation, Rev. Sci. Instrum. **87**, 093902 (2016).

[22] O. Arnold, J. C. Bilheux, J. M. Borreguero, A. Buts, S. I. Campbell, L. Chapon, M. Doucet, N. Draper, R. F. Leal, M. A. Gigg, V. E. Lynch, A. Markvardsen, D. J. Mikkelson, R. L. Mikkelson, R. Miller *et al.*, MANTID: Data analysis and visualization package for neutron scattering and μSR experiments, Nucl. Instrum. Methods A **764**, 156 (2014).

[23] R. A. Ewings, A. Buts, M. D. Le, J. van Duijn, I. Bustinduy, and T. G. Perring, HORACE: Software for the analysis of data from single crystal spectroscopy experiments at time-of-flight neutron instruments, Nucl. Instrum. Methods A **834**, 132 (2016).

[24] G. Kresse and D. Joubert, From ultrasoft pseudopotentials to the projector augmented-wave method, Phys. Rev. B **59**, 1758 (1999).

[25] G. Kresse and J. Furthmüller, Efficient iterative schemes for *ab initio* total-energy calculations using a plane-wave basis set, Phys. Rev. B **54**, 11169 (1996).

[26] J. P. Perdew, K. Burke, and M. Ernzerhof, Generalized Gradient Approximation Made Simple, Phys. Rev. Lett. **77**, 3865 (1996).

[27] H. J. Monkhorst and J. D. Pack, Special points for Brillouin-zone integrations, Phys. Rev. B **13**, 5188 (1976).

[28] S. L. Dudarev, G. A. Botton, S. Y. Savrasov, C. J. Humphreys, and A. P. Sutton, Electron-energy-loss spectra and the structural stability of nickel oxide: An LSDA+U study, Phys. Rev. B **57**, 1505 (1998).

[29] A. Togo and T. Tanaka, First principles phonon calculations in materials science, Scr. Mater. **108**, 1 (2015).

[30] O. V. Kovalev, *Irreducible and Induced Representations and Co-representations of Fedorov Groups* (Nauka, Moscow, 1986).

[31] M. N. Popova, E. P. Chukalina, T. N. Stanislavchuk, and L. N. Bezmaternykh, Different types of magnetic ordering in $RFe_3(BO_3)_4$, R = Gd, Tb, Er, and Y, as studied by the method of Er^{3+} spectroscopic probe, J. Magn. Magn. Mater. **300**, e440 (2006).

[32] S. Lovesey, *Theory of Neutron Scattering from Condensed Matter* (Oxford University Press, Fairlawn, NJ, 1984).

[33] B. Fåk and B. Dorner, Phonon line shapes and excitation energies, Phys. B (Amsterdam, Neth.) **234**, 1107 (1997).

[34] W. Cochran, Crystal stability and the theory of ferroelectricity, Adv. Phys. **9**, 387 (1960).

[35] A. D. Bruce and R. A. Cowley, Structural phase transitions III. Critical dynamics and quasi-elastic scattering, Adv. Phys. **29**, 219 (1980).

[36] J. A. Krumhansl and R. J. Gooding, Structural phase transitions with little phonon softening and first-order character, Phys. Rev. B **39**, 3047 (1989).

[37] R. A. Cowley, Soft modes and structural phase transitions, Integrated Ferroelectrics **133**, 109 (2012).

[38] W. Zhong, David Vanderbilt, and K. M. Rabe, First-principles theory of ferroelectric phase transitions for perovskites: The case of $BaTiO_3$, Phys. Rev. B **52**, 6301 (1995).

[39] S. K. Satija, S. M. Shapiro, M. B. Salamon, and C. M. Wayman, Phonon softening in $Ni_{46.8}Ti_{50}Fe_{3.2}$, Phys. Rev. B **29**, 6031 (1984).

[40] ISOTROPY Software Suite [http://iso.byu.edu].

[41] W. Setyawan and S. Curtarolo, High-throughput electronic band structure calculations: Challenges and tools, Comput. Mater. Sci. **49**, 299 (2010).